Eur. Phys. J. B **4**, 333–340 (1998)

THE EUROPEAN PHYSICAL JOURNAL B

Micelle-smectic phase coexistence: Origin of the maximum swelling of a mixed lamellar phase

F. Ricoul[1,a], M. Dubois[1], T. Zemb[1], and D. Plusquellec[2]

[1] Service de Chimie Moléculaire, bâtiment 125, CEA/Saclay, 91191 Gif-sur-Yvette, France
[2] E.N.S.C.R., avenue du Général Leclerc, 35700 Rennes, France

Received: 30 December 1997 / Accepted: 14 April 1998

Abstract. We use the water corner of the model ternary system water/DDAB (a cationic double tailed surfactant)/LS (an uncharged single chain glycolipid) to investigate maximum swelling of a charged lamellar phase. The phase diagram is determined by visual observation and small angle neutron scattering. Upon the addition of the glycolipid in this mixed lamellar structure, a decrease of the maximum swelling is observed. A transition from vesicles to micelles is also evidenced in the dilute coexisting phase. By calculating explicitly the osmotic pressure in the micellar phase and in the lamellar phase through the Poisson-Boltzmann equation, we demonstrate that equilibrium of the osmotic pressure in the two phases and depletion of the lamellar phase by the micellar phase explain quantitatively the decrease of maximum swelling observed when the LS to DDAB ratio increases.

PACS. 61.12.Ex Neutron scattering techniques (including small-angle scattering) – 64.70.Md Transitions in liquid crystals – 82.70.Dd Colloids

1 Introduction

In all the lamellar phases systems formed with surfactants, the maximum swelling of the lamellar phase, *i.e.* the maximum periodicity D_{max} of the smectic structure, has been described to be limited by different mechanisms.

- The most frequent case corresponds to the situation where the lamellar phase equilibrates with a very dilute monomer solution, *i.e.* when the osmotic pressure is close to zero at the maximum periodicity D_{max} of the lamellar phase. The zwitterionic phospholipid bilayer membranes are a classical example of this situation: as first shown by Parsegian *et al.* [1], at D_{max}, the short range repulsive force, also called "hydration" force, just counterbalances the van der Waals attractive force. Systematic measurements of maximum swelling, *i.e.* water layer thickness when the osmotic pressure vanishes, *versus* temperature, salt or dielectric constant of the polar layer is a simple, direct and convenient way to deduce the value of the Hamaker constant of such system [2].
- Another case occurs for instance in the case of the swollen pentaethylene glycol dodecylether $C_{12}E_5$ lamellar phase which contains up to 99% of water before demixing with an isotropic L_3 phase [3]. The measure of the maximum swelling D_{max} and of the coexisting persistence length would be an implicit way to measure the attractive force that counterbalances the Helfrich type long range repulsion that is usually assumed to be dominant [4].
- In the case of the charged DDAB (didodecyldimethylammonium bromide) bilayers, the maximum swelling of the lamellar phase L_α goes also up to $\sim 97.5\%$ of water which means that $D_{max} \sim 1000$ Å [5]. This corresponds to the appearance of a macroscopically homogeneous phase, noted $[L_\alpha]$, in which crystallites of lamellae coexist with closed onions like large vesicles (asymetric ${}^A L_3$ phase). This microphase separation is stable upon centrifugation of the sample and the two scattering signals are always superposed in a scattering experiment. The maximum swelling is thus related to the thermodynamical equilibrium between the two separated microphases, *i.e.* the equality of the osmotic pressure in the two phases: the electrostatic repulsion in the lamellar phase is equal to the entropic repulsion in the highly asymmetric L_3 phase (*cf.* [6]). An easy way to detect this situation is to demonstrate that the Bragg peaks do not move with water addition. This dilution with water mainly increases the relative fraction of vesicles *versus* the smectic part.

In any of these three cases maximum swelling of lamellar phases always corresponds to a plateau of the osmotic pressure in the biphasic region. And the value of D_{max} may be related to the value of the pressure in the dilute

[a] *Present address*: SPHA/LEPI, CEA/Valrhô, bâtiment 57, Marcoule, BP 171, 30207 Bagnols-sur-Cèze Cedex, France.
e-mail: `ricoul@genoise.cea.fr`

phase in coexistence with the lamellar phase and to the force balance involved.

In this article, our aim is to establish quantitatively the variation of the maximum swelling of the swollen DDAB lamellar phase upon the addition of a glycolipid in the charged cationic membrane. We use a synthetic uncharged single chain glycolipid, 2-O lauroylsaccharose [7].

2 Experimental

We use DDAB [$(CH_3)_2NBr(C_{12}H_{25})_2$] from Kodak recrystallized 3 times in ethyl acetate. 2-O Lauroylsaccharose [$(C_{13}H_{21}O_{12})(C_{11}H_{23})$], also noted LS in the following, has been synthesized as described previously [7]. Samples were dissolved in D_2O as received from Eurisotop. Characteristic physical quantities of both molecules are given in Table 1. The molecular volumes have been determined with a Density Measurement Apparatus DMA 60 from A. Paar (Graz, Austria). The critical micellar concentrations (cmc) have been deduced from surface tension measurements, with the drop weight method for DDAB and with a Digital-Tensiometer K10 (Krüss) using the so-called Du Nouy method with a ring for LS. The areas per head group have been deduced using Gibbs equation.

Samples were prepared in 4 ml culture glass tubes by weighting the desired amount of the different compounds and let equilibrate a few weeks. We define x_{LS} as the molar fraction of Lauroylsaccharose introduced in the DDAB bilayers: $x_{LS} = [LS]/([DDAB] + [LS])$.

In the case of demixtion after equilibration, coexisting phases in apparently homogeneous samples were separated by centrifugation during 12 hours at 4500 rpm. The water content was deduced from weight measurements before and after lyophilisation. The lyophilisat was redissolved in an equivolumic mixture of methanol and chloroform and the composition in surfactants, LS and DDAB, was given by quantitative Thin-Layer Chromatography-Flame Ionizable Detection Iatroscan technique (by Iatron, Tokyo, Japan). 1 μl of the solution was deposed with an "autospotter" on Silica-coated rods and eluted for 40 min in a 30:60:2.5:2 mixture of MeOH:$HCCl_3$:H_2O:NH_4^+aq. Calibration with pure DDAB and pure LS solutions was done separately. This procedure allows determination of composition of the two coexisting phases: the lamellar phase at the maximum swelling and the isotropic phase.

Small angle neutron scattering (SANS) analysis was performed in 1 or 2 mm quartz cells at the PAXE spectrometer (LLB, CEA Saclay, France). Three configurations were used: wavelength 5.5 Å and detector, uncentered, at 1.5 m and 5 m, and wavelength 14 Å, detector at 5 m so that the total q range that was investigated is $0.004 < q < 0.4$ Å^{-1}. The wavelength distribution set by the mechanical selector was $\Delta\lambda/\lambda \sim 10\%$. Intensities are given in absolute units (cm^{-1}) after a calibration with water (H_2O) was done in each configuration according to standard procedure [8].

Small angle X-ray scattering (SAXS) experiments were performed in cells with Kapton walls on the laboratory built Huxley-Holmes type pinhole collimation camera described in [9]. The data were recorded with a 2-D 33 cm diameter gas detector. The spatial resolution of this detector is 0.2 mm and the electronic background around 3 counts/pixel/hour [10].

The scattering intensity has been analyzed using different models. For independently oriented bilayers the intensity (in cm^{-1}) is given by:

$$I(q) = 2\pi\Phi\delta\frac{(\Delta\rho)^2}{q^2}\left(\frac{\sin q\delta/2}{q\delta/2}\right)^2 \quad (1)$$

where Φ is the volume fraction occupied by the bilayers, δ the bilayer thickness and $\Delta\rho$ the scattering length density difference between the bilayers and the solvent (D_2O).

To analyze micellar sample patterns we have used a program developed by Pedersen which enables to fit simultaneously SANS and SAXS data with least square method [11,12]. For ellipsoidal micelles, a two concentric shell model for the form factor is used that is expressed in function of the internal and external radii R_i and R_e, the scattering length densities ρ_i and ρ_e, and the ellipticity ε:

$$I(q, R_i, R_e, \varepsilon) = \Phi\int_0^{\pi/2} F^2[q, r(R, \varepsilon, \alpha)]\sin\alpha\ d\alpha \quad (2)$$

where

$$r(R, \varepsilon, \alpha) = R(\sin^2\alpha + \varepsilon^2\cos^2\alpha)^{1/2},$$

$$F(q, r) = \frac{1}{V}[\rho_i V(R_i) f(q, r_i) + (\rho_e - \rho_i)V(R_e)f(q, r_e)],$$

$$f(q, R) = \frac{3[\sin(qR) - qR\cos(qR)]}{(qR)^3}$$

and

$$V = \rho_i V(R_i) + (\rho_e - \rho_i)V(R_e)$$

if

$$V(R) = 4\pi R^3/3.$$

In the case of cylinders the expression for form factor includes a Bessel function of order one [11].

The structure factor is calculated analytically for spherical particles by solving the Ornstein-Zernike integral equation with an approximate closure relation. For uncharged micelles, *i.e.* for an hard sphere potential, we use the Percus-Yevick approximation. For charged micelles, a Hayter-Penfold calculation is followed with a Yukawa type electrostatic screened potential and a "Mean Spherical Approximation" and the renormalization of the hard sphere radius is done according to Hansen and Hayter [13]. For geometries other than spheres, the model does not allow explicit calculation of the structure factor. Therefore, only form factors are checked *versus* experiment for consistency.

The polar and apolar volumes as well as the scattering length densities used are given in Table 1. In the case of mixed samples, an average is done in the proportion of x_{LS}. Finally five free parameters are effectively used to fit the data: the aggregation number N, the hydration number h (*i.e.* the number of water molecules per surfactant included in the excluded volume), the ellipticity ε or

Table 1. Characteristic physical quantities and scattering length densities for the molecules used.

	DDAB		LS		D_2O
Molecular weight M (g/mol)	462		524		20
Critical micellar concentration (mol/l)	8×10^{-5}		6×10^{-4}		
Chain length l_c (Å)	11		15.4		
Area per head group s (Å^2)	65		65		
Packing parameter $p = V_{apol}/sl_c$	0.98		0.32		
	polar	apolar	polar	apolar	
Partial volume (Å^3/molecule)	84	700	372	323	30
$\rho_{neutron}(\times 10^{10}$ cm$^{-2})$	8.3	−0.39	4.7	−0.32	6.4

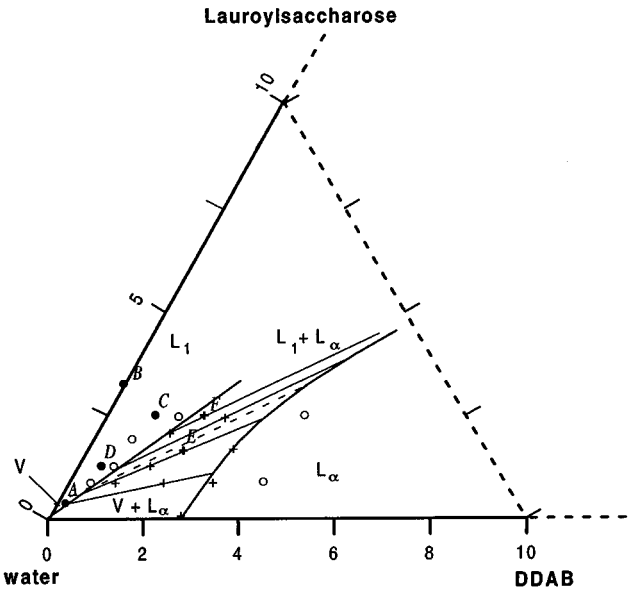

Fig. 1. Dilute part of the ternary phase diagram water/DDAB/2-O Lauroylsaccharose. The phases have been characterized both through visual observations and SANS analysis. Circles correspond to monophasic sample whereas crosses correspond to biphasic samples. V stands for the vesicle phase, L_1 for the micellar phase and L_α for the lamellar phase.

the cylinder length L, the hard sphere fraction ν_{HS} and the effective charge Z_{eff}. The same set of five parameters have to be consistent with the observed SANS and SAXS data [12,14]. Since only solutions corresponding to a possible packing of molecules of known volume, this procedure is more reliable than indirect Fourier transform method (*cf.* [15]).

3 Results

Figure 1 shows the dilute part of the ternary phase diagram of the water/DDAB/LS system. The symbols (circles and crosses) correspond to the samples that have been prepared at various compositions. They were first observed by eye between crossed polarisers. It was thus possible to distinguish between pure lamellar phase (permanently birefringent), highly asymmetric L_3 phase or vesicles (bluish and flow birefringent) or micellar phase (transparent, isotropic, or flow birefringent). The microstructures were then confirmed by SANS.

In Figure 2a we have plotted in logarithmic scale the SANS pattern of the sample noted A in Figure 1 ($x_{LS} = 0.42$, $\Phi_{surfactant} = 0.0056$). Four theoretical curves using different models are also plotted: the first one corresponds to the form factor of independent bilayers using $\Phi = 0.0056$, $\delta = 22$ Å and $\Delta\rho = 5.5 \times 10^{10}$ cm^{-2} in expression (1). The two following models correspond to spherical micelles, *cf.* equation (2), with an hard sphere potential and with a typical Yukawa potential: we kept $\Phi = 0.0056$ and we choose an aggregation number N of 75, an hydratation number of 15 and an ellipticity of 4. The last model corresponds to stiff uncharged cylinders: $N = 150$, $L = 800$ Å.

We see that the magnitude in cm^{-1} of the experimental data is only consistent with the hypothesis of bilayers. In Figure 2b, we have plotted the data on the representation adapted to flat objet, Iq^2 *versus* q. The oscillations at low angle are the result of the average spherical shape of the closed vesicles as well as the vesicle-vesicle repulsion interaction. We are here exactly in the situation described in full details by Oberdisse and Porte who demonstrated the existence of microvesicles [16]. Analysis of our data according to their method indicates us that we have microvesicles driven by charge stability, with a radius of 80 Å, a bilayer thickness of 22 Å and a distance between centers of 630 Å corresponding to the first peak in Figure 2b.

Figure 3 shows SANS and SAXS patterns for two samples, chosen in the micellar region and noted B (top) and C (bottom) in Figure 1. These samples correspond respectively to 4wt% of LS ($x_{LS} = 1$) and 3wt% LS + 1wt% DDAB ($x_{LS} = 0.75$). The SANS and SAXS spectra have been fitted simultaneously using the method described in the materials & method part and the final values of the fitting parameters are given in Table 2. The effective charge of the micelle C (0.12) is about one third of the value expected from the yet unique explicit analytical model

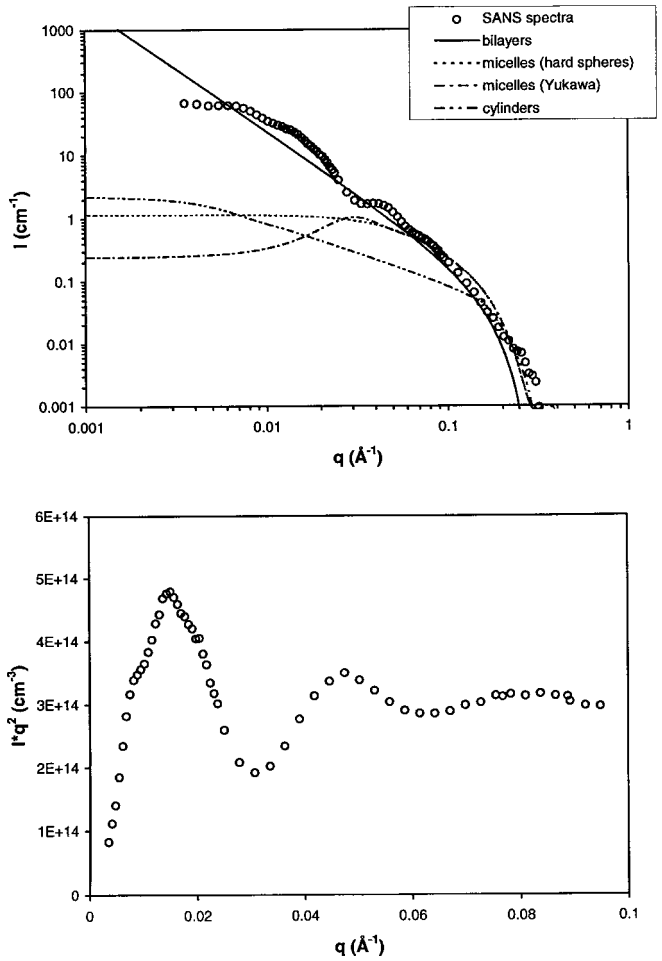

Fig. 2. (a) (top) Experimental SANS spectrum (circles) of the sample noted A in Figure 1, prepared in the vesicle phase domain ($x_{LS} = 0.42$, $\Phi_{water} = 99.44\%$ in volume). The lines correspond to 4 theoretical curves calculated for the scattering of bilayers, uncharged spherical or cylindrical micelles and charged spherical micelles. (b) (bottom) Iq^2 *versus* q representation of the SANS data of Figure 2a.

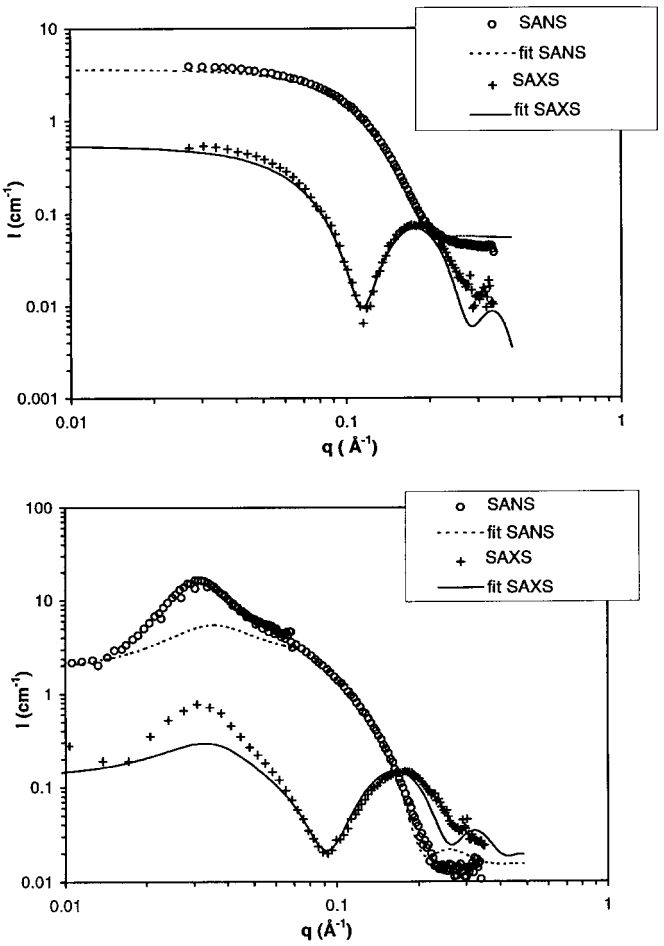

Fig. 3. Experimental SAXS (crosses) and SANS (circles) data of the samples noted B (top) and C (bottom) in Figure 1 and in the text. The curves correspond to the simultaneous SAXS and SANS fit using a two concentric ellipsoidal shells form factor model, with aggregation number, hydration number and ellipticity as parameters and a Hayter-Penfold calculation for the structure factor.

Table 2. Results of the fitting parameters for the mixed micelles.

Sample	B	C
DDAB (wt%)	0	1
LS (wt%)	4	3
$x_{LS} = [LS]/([DDAB] + [LS])$	1	0.75
Aggregation number $N_{DDAB+LS}$	76	77
Hydration number h	15	15
Ellipticity ε	1.4	1.3
Hard-sphere volume fraction ν_{HS}	0.032	0.1
Effective charge per surfactant Z_{eff}	10^{-5}	0.12

avaible in the litterature [17]. This dressed model predicts an effective charge characterized by a dissociation ratio effective charge/structural charge of 0.35. We note however that the difference in model prediction and observed value is close to the points obtained for the bromide counter ions in water (*cf.* Fig. 1 in Ref. [17]). In the mixed micelles described here, the bromide counter ion is in a sugar-water mixture having lower dielectric permittivity, thus reconciling the observed with theory. The hydration number (~ 15) is also higher than for ionic surfactants [18] but it is equal within 10% to other glycolipids studied in the literature [14,19].

We note that the values of the aggregation number, hydration number and ellipticity, do not change much between the pure LS micelle and the LS micelle with a significant molar fraction of DDAB molecules ($x_{LS} = 0.75$). This means that the difference in the packing parameters of the two molecules and the electric surface charge do not effect the globular shape of the micelles. From the value of

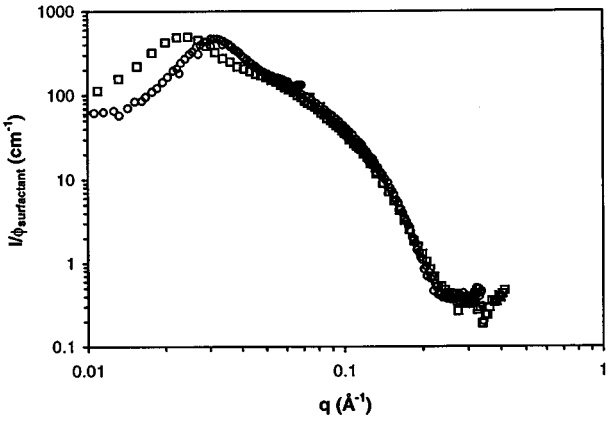

Fig. 4. SANS data, normalized by the total surfactant volume fraction, of the two micellar samples noted C (circles) and D (squares) in Figure 1. For both samples $x_{LS} = 0.75$, and $\Phi_{surfactant} = 0.035$ and 0.0175 respectively.

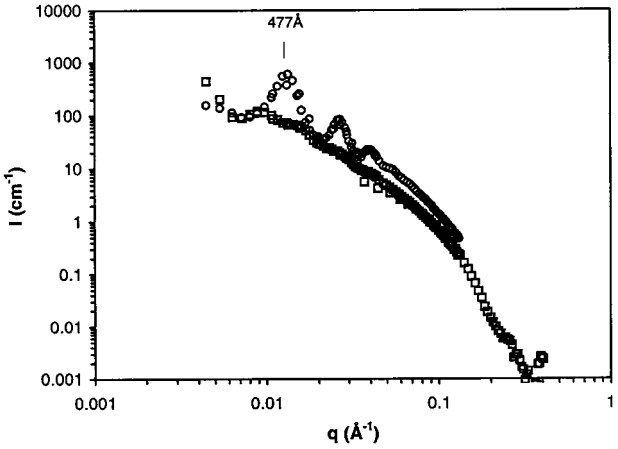

Fig. 5. SANS spectra of the upper, concentrated phase (circles) and the lower, dilute phase (squares) taken from the biphasic sample noted E in Figure 1: $x_{LS} = 0.47$, LS = 2wt%+$DDAB$ = 2wt%. This sample evidences a vesicle-lamellar coexistence.

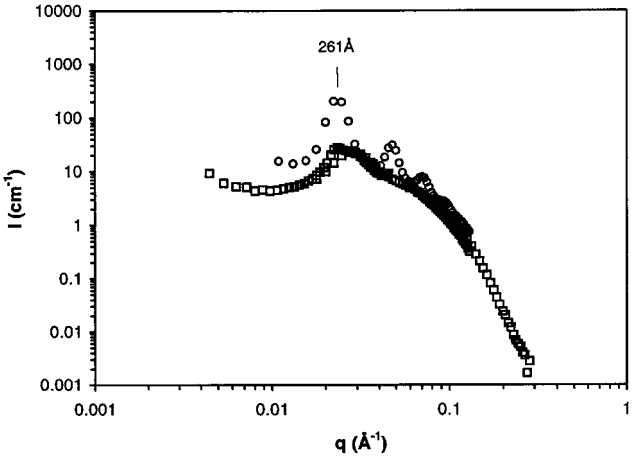

Fig. 6. SANS spectra of the upper, concentrated phase (circles) and the lower, dilute phase (squares) taken from the biphasic sample noted F in Figure 1: $x_{LS} = 0.5$, LS = 3wt%+$DDAB$ = 2wt%. In this case the lamellar (concentrated) phase coexists with a micellar phase.

the aggregation number it is possible to deduce the values of the interior (apolar) and exterior (effective value) radii, respectively 18 and 23.5 Å.

For the mixed micelle C (Fig. 3, bottom) we have observed that the model could not reproduce the strong interaction peak present at low q, even by varying the hard sphere radius. This may be explained by the fact that we use a $S(q)$ for spheres, and interaction in a set of charged spheres must underestimate the electrostatic interaction in elongated charged objects. But to our knowledge no simple analytic expression is available for ellipsoids. However the agreement at large q shows, specially for the SAXS data, on absolute scale, demonstrates that we have obtained small ellipsoidal micelles.

In Figure 4 we have plotted the scattering intensities of the samples C and D, normalized by the surfactant volume fraction. These two samples have been prepared with the same molar fraction of LS, $x_{LS} = 0.75$, D being two times more dilute than C. We note that at large q, the spectra stack perfectly which is a proof that the form factor of the micelles, *i.e.* their geometry, has not changed with the dilution. However the interaction peak has shifted, from $d = 203$ Å for C to 273 Å for D, which is a bit more that what is expected from the pure dilution effect ($\Phi \propto 1/d^3$). This is probably due to the influence of the form factor on the position of the weaker $S(q)$.

Samples noted E and F in Figure 1 are two phase samples, prepared in the biphasic region between the pure lamellar phase L_α and the pure dilute phase, that can be composed either by vesicles or by micelles, depending on x_{LS}. Figure 5 shows the SANS data of the upper, concentrated phase (circles) and lower, dilute phase (squares), after separation, of sample E. For the upper phase we recognize a series of several orders of Bragg peaks of a lamellar phase, with a periodicity of 477 Å. For the dilute phase, we observe a q^{-2} slope at low q which indicates that we have independent bilayers, like in Figure 2. In Figure 6 we have plotted the spectra of the concentrated and dilute phases of sample F. From the spectra we deduce that the concentrated phase is also a lamellar phase of lower periodicity, 261 Å, whereas the spectrum of the dilute phase has the same shape as the mixed micelles in Figure 3 or Figure 4.

From the analysis of all the samples in the biphasic region, we estimate the molar ratio composition of the lamellar phase at the stability limit to be $x_{LS} = 0.5$. This limit is represented by a dotted line in Figure 1 between samples where the lamellar phase demixes with a phase of vesicles and samples where the dilute phase in equilibrium with the lamellar phase could be identified as a micellar phase. Moreover the composition analysis by chromatography enabled us to draw the tie-lines between the coexisting phases. In the dilute isotropic phase, we have micelles at high LS content and vesicles at low LS content. Since micelles can penetrate the vesicles, these

samples never phase separate, as already been observed and discussed by others [20–22]. hence at low surface charge ($<$ 0.5 charge for $\sim$ 70 Å^2), the equilibrium is between a lamellar phase and micelles. At high surface charge ($>$ 0.5 charge for $\sim$ 70 Å^2) coexisting structures are a lamellar phase and vesicles. The value of $\overline{\kappa}$, the bending constant towards Gaussian curvature, become abruptly negative at high surface charge in the absence of salt [23, 24]. It is thus consistent to favor closed vesicles at higher surface charge in mixed systems. The same transition towards closed vesicles has been observed by Oberdisse *et al.* [16,20].

4 Discussion

As it can be observed in Figure 1, the maximum swelling of the lamellar phase diminishes as the molar fraction of LS, x_{LS}, increases, *i.e.* the lamellar region is reduced when we add the glycolipid. Particularly, the formation of the micelles instead of the vesicles increases the depletion of the lamellar phase, *i.e.* the maximum observable periodicity.

From the measurement of D_{max} by SANS, we can deduce the osmotic pressure in the lamellar phase at the limit of the demixtion. From earlier osmotic stress results obtained *via* the osmotic stress method, we know that the osmotic pressure in the swollen DDAB and mixed DDAB/glycolipid lamellar phases is dominated by the electrostatic repulsion [25]. Thus, it is possible to evaluate the osmotic pressure in the lamellar phase $\Pi_{L\alpha}$ by the asymptotic relation [26]:

$$\Pi(D_{max})_{L_\alpha} \approx 64kTc_s'\gamma^2 \exp(-\kappa' D_{max}) \qquad (3)$$

where k is Boltzmann's constant, T the temperature in degrees Kelvin, c_s' the salinity in a reservoir in equilibrium with the sample. In the case of DDAB, we found that the residual ion content after purification is slightly higher than the cmc of DDAB, so that $c_s' \approx 6\times10^{-4}$ mol/l, which correspond to an associated Debye length $1/\kappa'$ of 124 Å. The constant γ equals ~ 1 for highly charged membranes, approximately one structural charge every 70 Å^2 ($\sim$ 20 μC/cm^2). In Figure 7, we have thus plotted the osmotic pressure of the lamellar phase at the maximum swelling D_{max} calculated with equation (3) as a function of the molar fraction of x_{LS}. We note that the pressure increases quasi linearly with x_{LS} from very low pressures ($\sim$ 10 Pa) when the lamellar phase is in equilibrium with vesicles to higher pressures ($\sim$ 10 000 Pa) which correspond to the existence of the micellar phase.

Since there is a thermodynamical equilibrium between the lamellar phase and the dilute phase, the osmotic pressure in both phase must be the same. It is thus interesting to verify by calculation that the osmotic pressure of the dilute phase also increases with x_{LS}.

In the case of the charged micelles in the coexisting phase, (when $x_{LS} > 0.5$), since we have been able to characterize with a good precision, the size, the volume fraction and the charge of the micelles, it is possible to estimate theoretically the osmotic pressure using a Poisson-Boltzmann-Cell model for the spherical geometry [27]. The

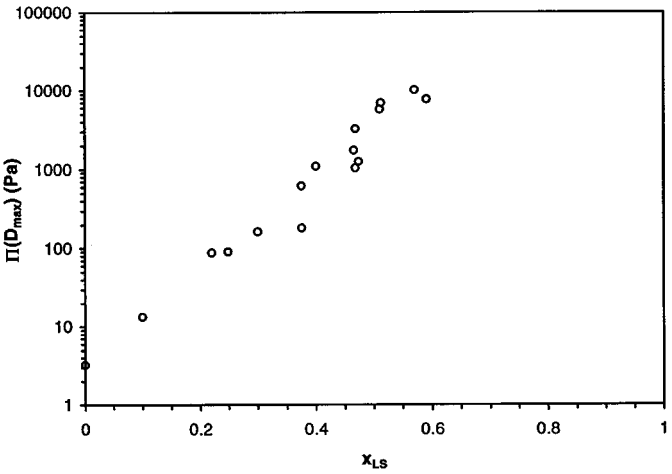

Fig. 7. Osmotic pressure of the lamellar phase at the maximum swelling versus the molar fraction x_{LS} of lauroylsaccharose added to the DDAB. The pressure was calculated using the experimental values of D_{max}, measured by SANS, in the asymptotic expression (3).

solution is divided in spherical, globally neutral, cells centered on the particles. The radius R of the cells is given by the micelle concentration, *i.e.* the surfactant volume fraction and the external radius ($\Phi_{surfactant} = (Re/R)^3$). The unlinearized Poisson-Boltzmann equation is solved numerically by iteration over the cell using the structural charge of the particles and the ionic profiles $c_+(r)$ and $c_-(r)$, of coions and counterions, are calculated around the colloidal particles. The osmotic pressure of the micellar phase can then be deduced by the results at the edge of the cell:

$$\Pi = kT(c_+(R) + c_-(R) - 2c_s') = 4kTc_s'\mathrm{sh}^2(\varphi(R)/2) \quad (4)$$

where c_s' is the salinity in the reservoir and φ is the normalized electrostatic potential. Generally, without added salt, the counterion contribution is dominant.

To apply this model to our micellar phase in equilibrium with the lamellar phase, we suppose, as shown in Figure 4, that the micelle structure does not vary with dilution. Therefore we did the calculation with the geometrical parameters of samples C and D, close to the demixtion line: radius = 23.5 Å, and a structural charge of $(1 - x_{LS})N = 21$. To avoid the problem of choosing arbitrary between constant potential or constant charge models, we have worked within the frame of the charge regulation model [28]. In the case of DDAB, we use a dissociation constant for the bromide of $pK = 0.95$, like what we have found in the case of the lamellar phase [25]. In Figure 8, the resulting pressure in the micellar phase, calculated with the Poisson-Boltzmann-Cell model, is plotted as a full line, *versus* the surfactant volume fraction. In particular we find that, for sample C, the pressure is 26 600 Pa and for sample D, 12 400 Pa.

In the same graph, we have also reported the osmotic pressure calculated in the lamellar phase, at the maximum swelling, using equation (3) and already shown in Figure 7. Since Bragg peaks are sharp, we neglect corrections due to fluctuations. Maximum swelling D_{max} has been converted

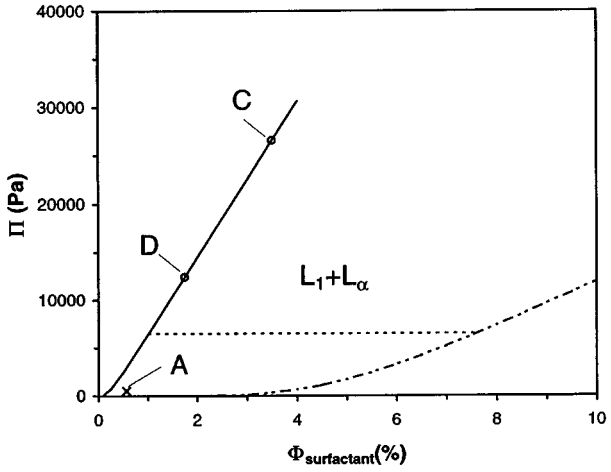

Fig. 8. Osmotic pressure of the mixed micelle phase (full line) calculated in function of the surfactant volume fraction using a Poisson-Boltzmann Cell model, with the hypothesis that the geometry of the micelles does not change with the dilution. The dotted curve corresponds to the osmotic pressure calculated for the lamellar phase, *i.e.* between two charged bilayers using the asymptotic expression (3), like in Figure 7.

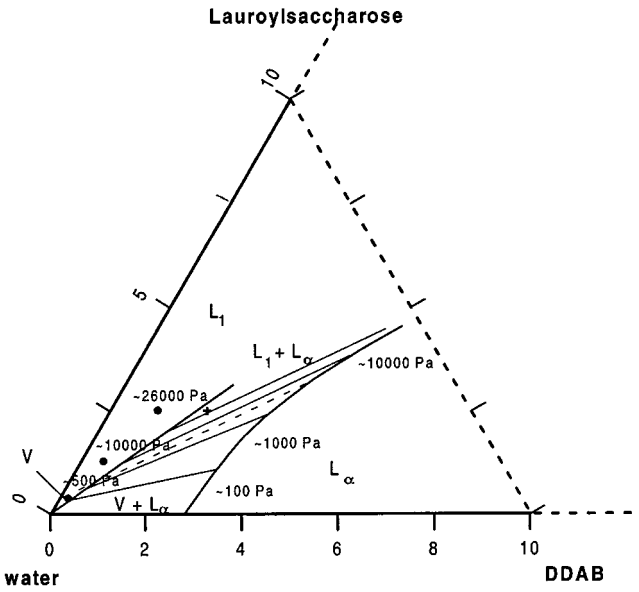

Fig. 9. Dilute part of the ternary phase diagram water/DDAB/2-O lauroylsaccharose, already shown in Figure 1. The indicated pressures correspond on one hand to the electrostatic plane-plane repulsion in the lamellar phase at the maximum swelling, and in the other hand to the Poisson-Boltzmann cell calculation in the micellar phase.

into the surfactant volume fraction using the simple relation: $\Phi_{surfactant} = \delta / D_{max}$. In Figure 8 we observe that the osmotic pressure increasing with the surfactant concentration is more important with the spherical geometry of micelles, than with the planar geometry of bilayers. For example the pressure calculated in the micellar phase with $\Phi_{surfactant} = 1\%$, 6360 Pa, corresponds to the osmotic pressure of a lamellar phase of periodicity $D_{max} \sim 320$ Å, *i.e.* at $\Phi_{surfactant} = 7.5\%$.

In Figure 9 we have also plotted the point that corresponds to sample A, composed of microvesicles and characterized in Figures 2a and b. The osmotic pressure has been evaluated approximately using the same Poisson-Boltzmann-Cell model as for the micelles. The microvesicles have been be considered as plain particles of radius 80 Å, with a maximum charge of 2200 (ratio of the external surface of the vesicle over the area per head group multiplied by $(1 - x_{LS})$), and with the same dissociation constant for the bromide as above, *i.e.* $pK = 0.95$. The volume fraction of the particles was taken equals to 0.0175 as the internal aqueous part of the vesicles is considered as part of the particle. Thus we find that the osmotic pressure is ~ 530 Pa, much lower that the pressure imposed in the micellar phase.

These values of the pressure, calculated in the dilute phase and in the lamellar phase at the maximum swelling, are consistent with the phase limits and the tie-lines of the experimental ternary phase prism that we have redrawn in Figure 9. We verify in this Figure 9 that the two phases in coexistence at both end of a tie-line have an osmotic pressure of the same order of magnitude. Thus the increase of the pressure from the vesicle phase to the micellar phase demonstrates that the lamellar phase in equilibrium is more and more depleted by the dilute phase when the molar fraction of glycolipid increases. There is a competition for water between the two phases. And the maximum swelling of the lamellar phase diminishes when the molar fraction of glycolipid increases.

5 Conclusion

Investigating the dilute part of the ternary phase diagram water/DDAB/LS, we have observed that the maximum swelling of the mixed DDAB/LS bilayers diminishes when the fraction of LS increases. This means that the osmotic pressure at the maximum swelling increases with x_{LS}. When $x_{LS} < 0.5$ we have observed that the dilute phase in equilibrium with the lamellar phase is composed of vesicles. When $x_{LS} > 0.5$ the single chained glycolipid, with a large polar volume, induces the formation of micelles in the dilute phase that equilibrates with a more concentrated lamellar phase. Since there is a two phase coexisting region, we have an osmotic equilibrium between the lamellar phase and the dilute phase. The explicit calculation of the osmotic pressure in the lamellar phase and in the dilute phase has demonstrated that the lamellar phase is depleted by the dilute phase and that the underlying mechanism of the maximum swelling is the competition for water between the two phases in equilibrium.

This behavior is a general behavior of the lamellar phase when it is in coexistence with micelles or any other competing phase. A miscibility gap with tie lines appears in the phase diagram. A difference in concentration of closed vesicles coexisting with the lamellar phase at maximum swelling explains the difference observed by Kunieda and Shinoda in the phase diagrams of DDABr

and DDACl [29,30]. Maximum concentration of DDAB vesicles is 0.15wt% whereas it is 0.6wt% for DDACl, corresponding to smaller vesicles for a less bound counter ion. The corresponding maximum swellings are > 700 Å for DDAB and 100 Å for DDACl. The pressure of the equilibrium plateau is respectively 300 Pa for DDAB [26] and is expected to be higher than 1000 Pa for DDACl [31]. We have also observed the same decrease of the maximum swelling with a double-tailed glycolipid added to the DDAB lamellar phase [32].

The authors wish to thank Luc Belloni for help in the osmotic pressure calculations, José Teixeira and Bruno Demé in the neutron scattering measurements, and Vance Bergeron in the DDAB surface tension measurements.

References

1. D.M. LeNeveu, R.P. Rand, V.A. Parsegian, D. Gingell, Biophys. J. **18**, 209-230 (1976).
2. L.J. Lis, M. McAlister, N. Fuller, R.P. Rand, V.A. Parsegian, Biophys. J. **37**, 657-666 (1982).
3. R. Strey, R. Schomächer, D. Roux, F. Nallet, U.J. Olsson, Chem. Soc. Faraday Trans. **86**, 2253-2261 (1990).
4. H. Bagger-Jörgensen, U. Olsson, Langmuir **12**, 4057-4059 (1996).
5. M. Dubois, Th. Zemb, Langmuir **7**, 1352-1360 (1991).
6. Th. Zemb, L. Belloni, M. Dubois, S. Marcelja, Prog. Colloid Polym. Sci. **89**, 33 (1992).
7. C. Chauvin, K. Baczko, D. Plusquellec, J. Org. Chem. **58**, 2291-2295 (1993).
8. B. Jacrot, Rep. Prog. Phys. **39**, 911-953 (1976).
9. V. Le Flanchec, D. Gazeau, J. Taboury, Th. Zemb, J. Appl. Cryst. **29**, 110 (1996).
10. F. Né, A. Gabriel, M. Kocsis, Th. Zemb, J. Appl. Cryst. **30**, 306-311 (1997).
11. J.S. Pedersen, Lecture notes for the *Third European Summer school on "Scattering Methods Applied to Soft condensed Matter"* (1996).
12. L. Arleth, D. Posselt, D. Gazeau, C. Larpent C., Th. Zemb, K. Mortensen, J.S. Perdersen, Langmuir **13**, 1887 (1997).
13. J.B. Hayter, J. Penfold, Molec. Phys **42**, 109 (1981); J.P. Hansen, J.B. Hayter, Molec. Phys. **46**, 651 (1982).
14. C. Cecutti, B. Focher, B. Perly, Th. Zemb, Langmuir **7**, 2580-2585 (1991).
15. L. Cantu, M. Corti, E. Del Favero, M. Dubois, Th. Zemb, Biophys. J (in press).
16. J. Oberdisse, G. Porte, Phys. Rev. E (in press).
17. J.B. Hayter, Langmuir **8**, 2873-2876 (1992).
18. Y. Chevalier, Th. Zemb, Rep. Prog. Phys. **53**, 279 (1990).
19. L. Cantu, M. Corti, E. Del Favero, M. Dubois, Th. Zemb, Langmuir (in press).
20. J. Oberdisse, O. Regev, G. Porte, J. Phys. Chem. B (in press).
21. E.Z. Radlinska, Th. Zemb, J.-P. Dalbiez, B.W. Ninham, Langmuir **9**, 2844-2850 (1993).
22. O. Söderman, K.L. Herrington, E.W. Kaler, D.D. Miller, Langmuir **13**, 5531-5538 (1997).
23. G. Porte, C. Ligoure, J. Chem. Phys. **102**, 4290-4298 (1995).
24. A. Fogden, J. Daicic, D.J. Mitchell, B.W. Ninham, Physica A **234**, 167-188 (1996); J. Daicic, A. Fogden, I. Carlsson, H. Wennerström, B. Jönsson, Phys. Rev. E **54**, 3984-3998 (1996); A. Fogden, J. Daicic, A. Kidane, J. Phys. II France **7**, 229-248 (1997).
25. F. Ricoul, M. Dubois, L. Belloni, Th. Zemb, C. André-Barrès, I. Rico-Lattes, Langmuir **14**, 2645-2655 (1998).
26. M. Dubois, Th. Zemb, L. Belloni, A. Delville, P. Levitz, R. Setton, J. Chem. Phys. **96**, 2278-2286 (1992).
27. L. Belloni, M. Drifford, P. Turq, Chem. Phys. **83**, 147-154 (1984); L. Belloni, Ph.D. Thesis, Paris VI University (1982).
28. B.W. Ninham, V.A. Parsegian, J. Theor. Biol. **31**, 405-428 (1971).
29. H. Kunieda, K. Shinoda, J. Phys. Chem. **82**, 1710-1714 (1978).
30. C. Kang, A. Khan, J. Colloid Interface Sci. **156**, 218-228 (1993).
31. M. Dubois, Th. Zemb, N. Fuller, R.P. Rand, V.A. Parsegian, J. Phys. Chem. B (in press).
32. F. Ricoul, Ph.D. Thesis, Paris VI University (1997), Ch. 5.